Bayesian location of the QCD critical point: a holographic perspective

Claudia Ratti[1,*], *Joaquin* Grefa[1,2], *Mauricio* Hippert[3], *T. Andrew* Manning[4], *Jorge* Noronha[5], *Jacquelyn* Noronha-Hostler[5], *Israel* Portillo Vazquez[1], *Romulo* Rougemont[6], and *Michael* Trujillo[1]

[1]Physics Department, University of Houston, Houston TX 77204
[2]Department of Physics, Kent State University, Kent, Ohio 44243, USA
[3]Department of Theoretical Physics, Rio de Janeiro State University, 20550-013 Rio de Janeiro, Brazil
[4]National Center for Supercomputing Applications, University of Illinois Urbana-Champaign, Urbana, IL 61801, USA
[5]Illinois Center for Advanced Studies of the Universe and Department of Physics, University of Illinois Urbana-Champaign, Urbana, IL 61801-3003, USA
[6]Instituto de Física, Universidade Federal de Goiás, Av. Esperança - Campus Samambaia, CEP 74690-900, Goiânia, Goiás, Brazil

Abstract. We present a Bayesian analysis, based on holography and constrained by lattice QCD simulations, which leads to a prediction for the existence and location of the QCD critical point. We employ two different parametrizations of the functions that characterize the breaking of conformal invariance and the baryonic charge in the Einstein-Maxwell-dilaton holographic model. They lead to predictions for the critical point that overlap at one sigma. While some samples of the prior distribution do not predict a critical point, or produce critical points that cover large regions of the phase diagram, all posterior samples present a critical point at chemical potentials μ_{Bc} ~550-630 MeV.

1 Introduction

Mapping out the QCD phase diagram is an open challenge in nuclear physics, which is the main program component of experiments such as STAR at the Relativistic Heavy-Ion Collider (RHIC) and CBM at FAIR [1]. In particular, while the phase transition between hadrons and quarks is a smooth crossover at low densities [2], several models predict the existence of a second-order critical point (CP), beyond which the transition becomes first order (for recent reviews see e.g.[3, 4]). In our analysis, we use a holographic approach [5] to extrapolate lattice QCD information from zero to large baryon chemical potential μ_B. This model is a natural good candidate, since it can reproduce lattice QCD results at low densities, where they are available [6, 7], and naturally leads to the almost ideal-fluid behavior of the Quark-Gluon Plasma [8], as observed in experiments. We use a Bayesian analysis, and two functional forms for the potential and coupling functions that are the main unknown in our model, to perform a systematic scan of the parameters, constrained by lattice QCD results at zero density [9, 10], with a probability given by the respective error bars. Our predictions for the QCD critical point, based on the posterior parameter distributions, agree within one sigma for the two model realizations, and collapse to a very small region of the phase diagram, which is within the phase transition band from lattice QCD simulations [11].

*e-mail: cratti@uh.edu

2 Einstein-Maxwell-Dilaton holographic model

The gauge/gravity duality provides a way to describe the physics of a thermal, strongly coupled field theory in 3+1 Minkowski space time in terms of dual black holes in a 4+1 dimensional asymptotically anti-de Sitter bulk spacetime.

We employ the following action, in which a Maxwell field A_μ is used to provide a description of a conserved charge in QCD, in our case baryon number, while a dilaton scalar field ϕ breaks conformal invariance. The action of our theory is given by

$$S = \frac{1}{2\kappa_5^2}\int_{\mathcal{M}_5} d^5\,\sqrt{-g}\left[R - \frac{(\partial_\mu\phi)^2}{2} - V(\phi) - \frac{f(\phi)F_{\mu\nu}^2}{4}\right], \tag{1}$$

where g is the determinant of the metric, R is the Ricci scalar, $F_{\mu\nu} = \partial_\mu A_\nu - \partial_\nu A_\mu$ is the Maxwell field strength, while $V(\phi)$ and $f(\phi)$ are functions tweaked to reproduce QCD physics at $\mu_B = 0$. The numerical solutions for the EMD fields in thermal equilibrium, generated by solving the bulk equations of motion for different pairs of initial conditions, are associated through the holographic dictionary with definite thermal states at the boundary QFT, corresponding to given values of temperature T and chemical potential μ_B. These functions are the central unknowns in our analysis, and we choose for them two ansätze as follows:

1. Polynomial-Hyperbolic Ansatz (PHA), a more common parametrization, similar to the one chosen in Ref. [6]

$$\begin{aligned} V(\phi) &= -12\cosh(\gamma\,\phi) + b_2\,\phi^2 + b_4\,\phi^4 + b_6\,\phi^6, \\ f(\phi) &= \frac{\mathrm{sech}(c_1\phi + c_2\phi^2 + c_3\phi^3)}{1+d_1} + \frac{d_1}{1+d_1}\mathrm{sech}(d_2\phi). \end{aligned} \tag{2}$$

2. Parametric Ansatz (PA), a parametrization where it is more straightforward to relate the parameters directly to plateaus and exponential slopes in the potential [11]

$$\begin{aligned} V(\phi) &= -12\cosh\left[\left(\frac{\gamma_1\,\Delta\phi_V^2 + \gamma_2\,\phi^2}{\Delta\phi_V^2 + \phi^2}\right)\phi\right], \\ f(\phi) &= 1 - (1-A_1)\left[\frac{1}{2} + \frac{1}{2}\tanh\left(\frac{\phi-\phi_1}{\delta\phi_1}\right)\right] + -A_1\left[\frac{1}{2} + \frac{1}{2}\tanh\left(\frac{\phi-\phi_2}{\delta\phi_2}\right)\right]. \end{aligned} \tag{3}$$

3 Bayesian analysis and results

We will scan the parameter space for the two ansätze described above, in order to generate an ensemble of models distributed according to the error bars on lattice QCD results. We use Bayes theorem to find the posterior distributions for the model parameters, $\vec{\theta}$, given the lattice QCD constraints $\vec{d}$ as follows

$$P(\vec{\theta}|\vec{d}) = \frac{P(\vec{d}|\vec{\theta})P(\vec{\theta})}{P(\vec{d})} \tag{4}$$

where $P(\vec{\theta})$ is the prior probability distribution for the model parameters, and we treat $P(\vec{d})$, known as the evidence, as a normalization factor for the posterior.

To locate the critical point, we look at lines of constant ϕ_0 while increasing Φ_1, where ϕ_0 and Φ_1 are the values of the dilaton and $U(1)$ electric fields at the event horizon of a black hole solution, which correspond to the two initial conditions needed to numerically solve the

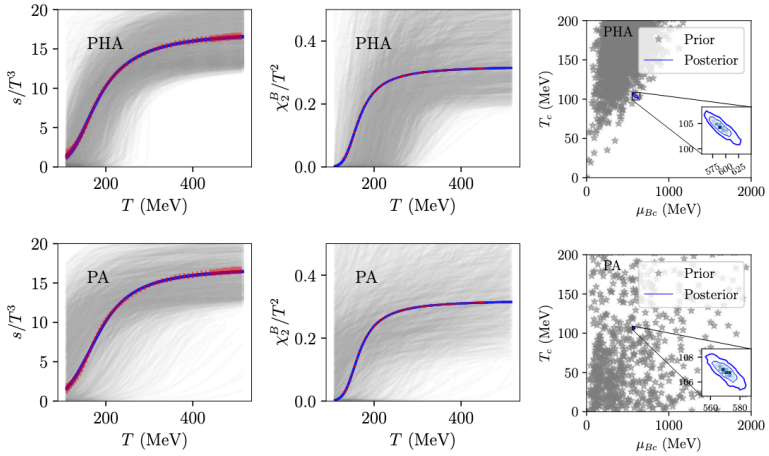

Figure 1. Results for sample equations of state from the prior (gray) and posterior (blue) distributions, for the PHA (top) and PA (bottom) Ansätze. Left: normalized entropy density vs temperature. Center: normalized baryon susceptibility vs temperature. Right: Predictions for the QCD critical point for the prior (grey stars) and posterior samples (blue histogram and contours). In the left and center panels, the red points with error bars are the lattice results from Refs. [9, 10]. In the rightmost panels, the blue lines visible in the inset represent 68% and 95% confidence levels for the posterior distribution.

bulk field equations. These lines are parallel at $\mu_B = 0$, but they cross at the CP and lead to a three-solution region beyond it.

The gray lines in the leftmost and middle panels of Fig. 1 display the prior equations of state, resulting from the functions $f(\phi)$ and $V(\phi)$ utilized in our analysis. The rightmost panels show the spatial distribution of critical points in the (T, μ_B) plane corresponding to these samples of the priors. The top and bottom panels correspond to the PHA and PA models, respectively. While $\sim$ 20% of the prior sample does not produce a critical point at all for the PA model, critical points found in this sample are scattered over a very wide region in the phase diagram. On the other hand, the prior for the PHA version of the model comparatively produces critical points that are concentrated mainly in one region of the phase diagram.

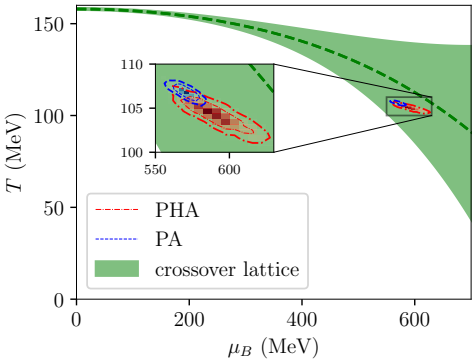

Figure 2. Predictions for the critical point location on the (T, μ_B)-plane, based on the posterior distributions for the PHA model (red) and the PA model (blue). Also shown is the extrapolation of the lattice QCD transition line from Ref. [12] (green band), based on the peak of the chiral susceptibility. Lines around confidence regions for the critical point location represent 68% and 95% confidence levels.

Figure 2 shows that the predicted distributions for the critical point location from our Bayesian analysis for the PHA (red) and PA (blue) Ansätze, are located within a narrow region in T and μ_B. Moreover, the regions for the PA and PHA Ansätze agree, with overlapping 68% confidence regions. For a posterior distribution of the parameter values see Ref. [11].

4 Conclusions

We have presented results for the first Bayesian analysis of the phase diagram of QCD constrained by first-principles lattice QCD results at zero baryon density. The posterior distribution of CP locations was computed for two different parametrizations of a holographic EMD model. We find that imposing agreement with lattice QCD tightly constrains predictions for the QCD CP location, which were spread all around the phase diagram in the unconstrained prior. Moreover, bands for the CP location within each model overlap within one sigma, indicating the robustness of our results against parametrization choices.

5 Acknowledgements

This material is based upon work supported in part by the National Science Foundation within the framework of the MUSES collaboration, under grant number No. OAC-2103680, as well as under grants No. PHY-2208724, PHY-1748958 and PHY-2116686, in part by the U.S. Department of Energy, Office of Science, Office of Nuclear Physics, under Award Number DE-SC0022023, DE-SC0023861, as well as by the National Aeronautics and Space Agency (NASA) under Award Number 80NSSC24K0767. The authors also acknowledge support from the Illinois Campus Cluster, a computing resource that is operated by the Illinois Campus Cluster Program (ICCP) in conjunction with the National Center for Supercomputing Applications (NCSA), and which is supported by funds from the University of Illinois at Urbana-Champaign. R.R. acknowledges financial support by National Council for Scientific and Technological Development (CNPq) under grant number 407162/2023-2.

References

[1] A. Lovato, *et al.* [arXiv:2211.02224 [nucl-th]].

[2] Y. Aoki, G. Endrodi, Z. Fodor, S. D. Katz and K. K. Szabo, Nature **443** (2006), 675-678.

[3] A. Bzdak, S. Esumi, V. Koch, J. Liao, M. Stephanov N. Xu, Phys. Rept. **853** (2020), 1-87

[4] L. Du, A. Sorensen and M. Stephanov, [arXiv:2402.10183 [nucl-th]].

[5] R. Rougemont, J. Grefa, M. Hippert, J. Noronha, J. Noronha-Hostler, I. Portillo and C. Ratti, Prog. Part. Nucl. Phys. **135** (2024), 104093

[6] R. Critelli, J. Noronha, J. Noronha-Hostler, I. Portillo, C. Ratti and R. Rougemont, Phys. Rev. D **96** (2017) no.9, 096026

[7] J. Grefa, J. Noronha, J. Noronha-Hostler, I. Portillo, C. Ratti and R. Rougemont, Phys. Rev. D **104** (2021) no.3, 034002

[8] J. Grefa, M. Hippert, J. Noronha, J. Noronha-Hostler, I. Portillo, C. Ratti and R. Rougemont, Phys. Rev. D **106** (2022) no.3, 034024

[9] S. Borsanyi, Z. Fodor, C. Hoelbling, S. D. Katz, S. Krieg and K. K. Szabo, Phys. Lett. B **730** (2014), 99-104

[10] R. Bellwied, S. Borsanyi, Z. Fodor, S. D. Katz, A. Pasztor, C. Ratti and K. K. Szabo, Phys. Rev. D **92** (2015) no.11, 114505

[11] M. Hippert, J. Grefa, T. A. Manning, J. Noronha, J. Noronha-Hostler, I. Portillo Vazquez, C. Ratti, R. Rougemont and M. Trujillo, Phys. Rev. D **110**, no.9, 094006 (2024)

[12] S. Borsanyi, Z. Fodor, J. N. Guenther, R. Kara, S. D. Katz, P. Parotto, A. Pasztor, C. Ratti and K. K. Szabo, Phys. Rev. Lett. **125** (2020) no.5, 052001